Honor Thesis

SELECTION RULES AND POPULATION TRAPPING IN RYDBERG STATES IN STRONG FIELD INTERACTIONS

Zetong Xue

Thesis Defense Committee

Dr. Andreas Becker	Advisor	Department of Physics
Dr. Agnieszka Jaron-Becker	Faculty Member	Department of Physics
Dr. William DeMeo	External Faculty Member	Department of Mathematics
Dr. Daniel Dessau	Honors Council Representative	Department of Physics

Thesis directed by Prof. Andreas Becker

Ultrafast AMO Theory Group

JILA and Department of Physics

University of Colorado at Boulder

October 31, 2018

Abstract

We study the excitation to Rydberg states in the interaction of the hydrogen and helium atom with a short strong laser pulse, as it has been analyzed before for monochromatic cw lasers. Utilizing solutions of the time-dependent Schrödinger equation we have analyzed if the parity of the populated angular momentum states agrees with the selection rules for multiphoton resonant absorption. We have further investigated how the results and conclusions depend on the parameters of the laser pulse, such as intensity and pulse length. Different mechanisms to explain the distributions in the populations of the angular momentum states are tested by our simulations.[1]

Keywords: atomic, molecular and optical physics; strong-field physics; attosecond physics; excitation; population trapping; selection rules.

[1]The work presented in this thesis is part of a project, in which the contributors were supported by grants from the U.S. National Science Foundation (Grant No. PHY-1734006), the U.S. Department of Energy, Division of Chemical Sciences, Atomic, Molecular and Optical Sciences Program (Award No. DE-SC0001771) and AFOSR MURI (Grant No. FA9550-16-1-0121). We utilized the JILA compute cluster Terra and the RMACC Summit supercomputer, which is supported by the National Science Foundation (Award No. ACI-1532235 and No. ACI-1532236), the University of Colorado Boulder, and Colorado State University. The Summit supercomputer is a joint effort of the University of Colorado Boulder and Colorado State University.

Acknowledgements

Truly thank you to my parents, I wasn't an easy kid growing up, in fact, I was the most troubled kid around, but luckily my parents had incredible patience and wisdom and been helping me financially and mentally as much as they could. Now I look back to them, I realize it was extremely difficult to support me all the way to today's stage, I can never forget the story that they spent all their savings just to buy me the best milk powder in the store when we were not financially comfortable; they put me and my education above all else and they are my most beloved people who got me into Physics and Mathematics and taught me how to be a righteous person.

Thank you to both of my loving grandparents, I spent a great deal of childhood time with them, and that time was one of my best memories. Every day I wish I could go back to that simple time so I can taste my grandma's cooking or play with the wooden sword and the catapult that my grandpa made for me. Every night I dreamt I can go back to that village so I can again steal neighbors' vegetables and end up being chased by their dogs, or climb up to the top of the mountain in the morning to see the sunrise from the sea.

Many thanks to my cousins PengFei and ShaoJun, they are my best friends and been supporting me ever since. Although we were not born on the same day, I wish I could ride crane with them to heaven on the same day when the time comes. Thanks to my aunts and uncles, we are very close and they have been, and are continuously supporting me.

Special thanks to Ultrafast AMO Theory Group, especially Prof. Andreas Becker, who not only taught me valuable classes and has been giving me incredible moral supports, but also gave me wonderful research opportunities and very patiently passed down his wisdom to me. From him, I learned how to do research, how to work collaboratively, and how to turn my passion into scientific results, not to mention all the Strong Field theory I learned from him. I can't thank him enough. Also special thanks to Joel, who I bothered over a trillion times and has been patiently helping me to conduct my research; his help was crucial to me. Thank you to Brynn for reviewing my works. Also thanks to Prof. Agnieszka Jaron-Becker, who has been supporting me over the years and thank you to Brynn, Cory, Tennesse, Andres and Andrew for making the group feel like home.

Thanks to Prof. Andreas Becker, Prof. Agnieszka Jaron-Becker, Prof. Daniel Dessau, and Prof. William DeMeo for agreeing to preside on my thesis committee. Thank you to Prof. Daniel Dessau who leads a wonderful honor class, and thank you to Prof. William DeMeo who taught one of the best math classes

I have ever had and gave me many supports to pursue the Mathematics that even outside of the class content.

Finally, Thank you to TianYi, who has been supporting me and overly praising my intelligence and who I had many very insightful conversations about Physics, Mathematics, and life. Thank you to Parker, who made my undergraduate life much more vibrant. Thank you to Prof. Thomas Schibli and Prof. Shijie Zhong for valuable classes and advise. Thanks to all the Peking Operas and Kunqu that accompanied me every sleepless night. Also thanks to Lao Tzu and Chuang Tzu, whose philosophy guides me in every aspect of my life.

Glossary

H	Hilbert space.
$\epsilon_0 = 8.85419 \times 10^{-12} F\ m^{-1}$	Permittivity of free space.
$\hat{H}$	Hamiltonian operator.
$\hbar = 1.05457 \times 10^{-34} J\ s$	Planck constant/2π.
$\mathbb{C}$	Complex Number Set.
$\mathbb{N} = \{1, 2, 3...\}$	Natural Number Set.
$\mathbb{R}$	Real Number Set.
$\mu_0 = 1.25664 \times 10^{-6} H\ m^{-1}$	Permittivity of free space.
$e = 1.60218 \times 10^{-19} C$	Elementary charge.
$m_e = 9,10938 \times 10^{-31} C$	Electron mass.
$m_p = 1.67262 \times 10^{-27} C$	Proton mass.

Contents

1 Introduction **3**

2 Theory **5**

2.1 Preliminaries 5

2.1.1 Electrodynamics 5

2.1.2 Quantum mechanics 5

2.1.3 Energy levels of hydrogen-like atoms 6

2.1.4 Semi-classical field interaction 8

2.2 Interaction of atoms with laser pulses 9

2.2.1 First order perturbation theory and selection rules 9

2.2.2 Multiphoton processes 12

2.2.3 Strong field interaction 12

2.2.4 Numerical methods 14

3 Results and Discussion [2] **16**

3.1 Selection rules for multiphoton processes 17

3.1.1 Generalization of selection rules for multiphoton processes 17

3.1.2 Selection rules: Parity effect in interaction with pulses 18

3.1.3 Dependence on intensity and pulse length 21

3.2 Population trapping 23

3.2.1 Resistance to ionization for high l states 23

3.2.2 Trapping in lower excited states 24

4 Summary and future goals **27**

Bibliography **28**

[2] Part of the results presented also appeared in J. Venzke, R. Reiff, Z. Xue, A. Jaroń-Becker and A. Becker, *Angular momentum distribution in Rydberg states excited by a strong laser pulse*, Phys. Rev. A **98**, 043434 (2018).

Chapter 1

Introduction

A single electron atom, at first glance, has a simple structure: a core with one electron. But as we dive into the details, we will discover a complex and dynamic structure of energy levels. Since an atom is too small to be observed directly, we have to use indirect methods to investigate the properties and structure of such atoms; it is not surprising that lasers provide us a good way to probe those atoms: lasers interact with the electrons and change the structure of energy levels; most importantly, lasers are sources of highly coherent light, making them an ideal tool for extracting information from an atom (molecule, etc.) or preparing the initial state of an atom in an experiment.

The theory of strong field physics is relatively new, and promising, but the theory of light-atom interaction can be traced back to early 20th century. From Dirac's golden rule [1] to Einstein's derivation of spontaneous emission [2], the theory of the interaction of an atom with light began to shine. More recently, scientists have been creating shorter and stronger laser pulses to probe more and more details of the atom in order to extract more information and achieve more applications. One part of the Nobel Prize in Physics in 2018 has recently been awarded to Prof. Gerard Mourou and Prof. Donna Strickland for their method of generating high-intensity, ultra-short optical pulses [3]. In 2001, research groups at Commissariat à l'Energie Atomique (CEA), Saclay (Paris, France) [4] and at the Technical University of Vienna (Austria) [5] produced the first attosecond (1 as = 10^{-18} s) laser pulses by using high harmonic generation (see details of the high harmonic generation process in section 2.2.3). The development of attosecond laser pulses has opened the way to the investigation of ultrafast processes at the level of electrons in many fields of science.

Under strong and short fields, processes become highly non-linear and induce some surprising phenomena. Consequently, the interaction of the electron with the intense light field cannot be described using perturbation theory, the theoretical approach that we learn in our quantum mechanics courses.

With such short pulses, we can retrieve more detailed information about atoms that was not previously obtainable with other imaging processes; with help of ultrafast pulses, the Auger decay time [6] and autoionization lifetime [7] can be measured directly.

In this thesis, we have studied the angular momentum distribution in an atom excited under such short and strong pulses. We have discovered rather surprising and interesting phenomena, namely the selection rule, which we know for perturbative single-photon processes, often holds for multiphoton processes in strong fields as well, even when the interaction becomes non-perturbative. Furthermore, we propose a population trapping mechanism, which prevents electrons from populating highly excited states with low angular momentum. In the remainder of the thesis, we will first introduce theory preliminaries that are required to explain strong field physics. Then, we present and investigate the numerical results, obtained by solving the Schrödinger equation on the computer, and discuss under which conditions the selection rule holds in strong fields (section 3.1) and the population trapping mechanism (section 3.2) .

Chapter 2

Theory

2.1 Preliminaries

2.1.1 Electrodynamics

The details of a more rigorous introduction to Quantum Mechanics and Electrodynamics can be found in [8, 1, 9], here we restate the fundamental Maxwell equations:

$$\nabla \cdot \mathbf{B} = 0,$$

$$\nabla \times \mathbf{B} = \mu_0 \left(\mathbf{J} + \epsilon_0 \frac{\partial E}{\partial t} \right),$$

$$\nabla \cdot \mathbf{E} = \frac{\rho}{\epsilon_0},$$

$$\nabla \times \mathbf{E} = \frac{\partial \mathbf{B}}{\partial t},$$

where $\mathbf{B}, \mathbf{E}, \mathbf{J}, \rho, \mu_0$, and ϵ_0 stand for the magnetic field, electric field, current density, charge density, permeability of free space, and permittivity of free space, respectively. This report uses semi-classical theory, which means the dynamics of the laser field follows Maxwell equations, while we treat particles quantum mechanically.

2.1.2 Quantum mechanics

In early 20th century, the equations that govern the dynamics of electrons in matter via the description of quantum states (non-relativistic single particles) were discovered. The time evolution of a state in

the Hilbert space $|\Psi(\mathbf{r},t)\rangle \in H$, is governed by the Schrödinger equation as:

$$i\hbar\frac{\partial}{\partial t}|\Psi(\mathbf{r},t)\rangle = \left[\frac{\hat{P}^2}{2m} + \hat{V}(\mathbf{r},t)\right]|\Psi(\mathbf{r},t)\rangle \ , \tag{2.1}$$

where $\hat{P}$ is the momentum operator, given by $\hat{P} = -i\hbar\nabla$ in the position basis. Alternatively, if we can employ the Heisenberg picture in which the operators $\hat{A}(t)$ are the dynamical objects (while the quantum states do not vary with time):

$$\frac{d}{dt}\hat{A}(t) = \frac{i}{\hbar}\left[\hat{H},\hat{A}(t)\right] + \left(\frac{\partial A}{\partial t}\right)_H \ , \tag{2.2}$$

where $[\cdot,\cdot]$ is the standard Lie bracket (or the commutator), $\hat{A}$ is the operator of some physical observable such as momentum, parity, energy etc. and $\hat{H}$ is the Hamiltonian operator (which usually corresponds to energy of the state). The latter is defined, for any quantum eigenstate (or eigenvector) in the Hilbert space $|E_i\rangle \in H$ with the energy $E_i \in \mathbb{R}$, as:

$$\hat{H}|E_i\rangle = E_i|E_i\rangle. \tag{2.3}$$

In this thesis, we are going to focus on the Schrödinger picture, since it is most convenient one for the description of the interaction of atoms with (strong) light fields.

2.1.3 Energy levels of hydrogen-like atoms

We know that the hydrogen atom consists of one proton with charge +e ($\approx 1.6 \times 10^{-19}$ C) and one electron with charge -e. Furthermore, the positively charged proton will attract the negatively charged electron, with the force between being the Coulomb force, and the corresponding potential is (in spherical coordinates):

$$\hat{V}(\mathbf{r}_N - \mathbf{r}_e) = -\frac{e^2}{4\pi\epsilon_0|\mathbf{r}_N - \mathbf{r}_e|},$$

where $\mathbf{r}_N$ and $\mathbf{r}_e$ are the positions of the proton and the electron, respectively. Using center-of-mass and relative coordinates, this two particle system can be transferred into a one particle system with the effective potential

$$\hat{V}_{eff} = \hat{V}(\mathbf{r}) + \frac{\hbar^2 l(l+1)}{2\mu r^2} \tag{2.4}$$

where $\hbar$ is the reduced Planck's constant, l being the angular momentum of the electron and the reduced mass $\mu = \frac{m_e m_p}{m_e+m_p}$. m_e and m_p stand for the mass of the electron and proton, respectively. Using single

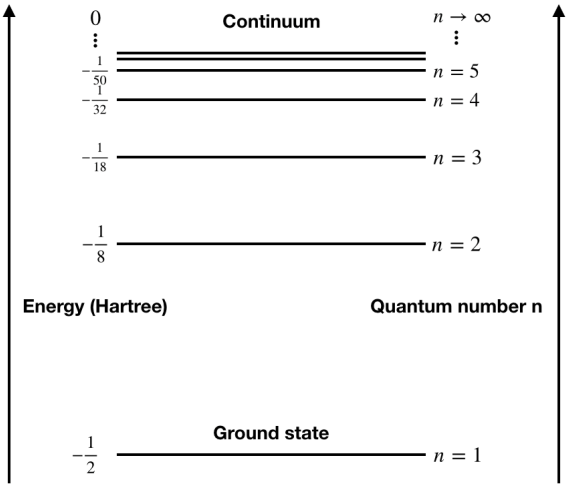

Figure 2.1: Energy spectrum of the bound states in the hydrogen atom.

particle quantum mechanics we can write the Hamiltonian in spherical coordinates as:

$$\hat{H}_0 = \frac{\hat{P}^2}{2m} + \hat{V}_{eff} = -\frac{\hbar^2}{2\mu r^2}\frac{d}{dr}\left(r^2\frac{d}{dr}\right) + \hat{V}(\mathbf{r}) + \frac{\hbar^2 l(l+1)}{2\mu r^2} \tag{2.5}$$

and, hence, the Schrödinger equation as

$$i\hbar\frac{\partial}{\partial t}|\Psi(\mathbf{r},t)\rangle = \left[\frac{\hat{P}^2}{2m} + \hat{V}(\mathbf{r})\right]|\Psi(\mathbf{r},t)\rangle = \left[-\frac{\hbar^2}{2\mu r^2}\frac{d}{dr}\left(r^2\frac{d}{dr}\right) - \frac{e^2}{4\pi\epsilon_0 r} + \frac{\hbar^2 l(l+1)}{2\mu r^2}\right]|\Psi(\mathbf{r},t)\rangle \tag{2.6}$$

The actual solution method is complex but given in many standard quantum mechanics textbooks, so we will state the result here, for the details, see e.g. [10]. For hydrogen atom, there exist discrete levels with negative energy, the electron can occupy to form a bound atom. These states are given by (for convenience, we will now also use Hartree atomic units, $\hbar = e = m_e = 1$):

$$E_n = -\frac{1}{2n^2}\left(\frac{e^2}{4\pi\epsilon_0}\right)^2\frac{\mu}{\hbar^2} = -\frac{1}{2n^2}\ , \tag{2.7}$$

where $n \in \mathbb{N}$. Figure 2.1 shows the energy level structure of the bound states in the hydrogen atom.

Furthermore, for each quantum number n, we have another two sets of quantum numbers l and m, which must satisfy $l \in \{0, 1, 2, ..., n-1\}$, and $m \in \{-l, ..., l\}$. The quantum number l describes the angular momentum of the state and m describes the projection of angular momentum to a particular direction (for example, the z direction in Cartesian coordinates). A given energy level in the hydrogen atom is degenerate with respect to the quantum numbers l and m.

The full set of quantum numbers n,l, and m represents a spinless particle state in Hilbert space (the property spin is the intrinsic angular momentum of a particle), since $\{|nlm\rangle\}$ form an orthonormal basis

set of Hilbert space:

$$\langle n'l'm'|nlm\rangle = \delta_{n'n}\delta_{l'l}\delta_{m'm} \ , \tag{2.8}$$

and these are simultaneous eigenvectors of $\hat{H}$, $\hat{L}^2$, and $\hat{L}_z$, i.e. the standard Lie bracket (or the commutator) of any two of the three operators vanishes:

$$[\hat{H}, \hat{H}] = [\hat{H}, \hat{L}^2] = [\hat{H}, \hat{L}_z] = [\hat{L}^2, \hat{L}_z] = 0. \tag{2.9}$$

From the Heisenberg picture, Equation (2.2), we can therefore conclude that the three physical corresponding observables are independent of time. And, $|nlm\rangle$ are hence eigenstates of the Hamiltonian, also called stationary states.

2.1.4 Semi-classical field interaction

To explore the interaction of intense laser radiation with atoms, we treat the electromagnetic field classically, governed by the Maxwell equations, and the particle quantum mechanically. The Schrödinger equation for a hydrogen-like one-electron system interacting with an external laser pulse, represented by the quantum state $|\Psi(\mathbf{r}, t)\rangle$, is then given by:

$$i\hbar\frac{\partial}{\partial t}|\Psi(\mathbf{r}, t)\rangle = \left[\frac{1}{2m}\left(-i\hbar\nabla + e\mathbf{A}(\mathbf{r}, t)\right)^2 - \frac{Ze^2}{(4\pi\epsilon_0)r}\right]|\Psi(\mathbf{r}, t)\rangle \ , \tag{2.10}$$

where Z is the number of protons in the atom, i.e. for hydrogen atom, $Z = 1$, hydrogen-like ion He^+ (two protons and one electron), $Z = 2$, etc.. For the case of helium atom, that we also study below, we use so-called single-active-electron potentials, in which all but one electron of an atom are assumed to be frozen.

In general, whether or not Equation (2.10) can be solved analytically depends on the form of $\mathbf{A}(\mathbf{r}, t)$ we apply. Typically, atomic wave functions extend over distances of about one Angström, meanwhile the fields we apply usually have wavelengths of several thousand Angström. Thus, we can treat the field across the atom as a function of time only, independent of the spatial variables. This gives us the so-called dipole approximation (for details on dipole approximation, see [2]).

2.2 Interaction of atoms with laser pulses

2.2.1 First order perturbation theory and selection rules

For the general form of electromagnetic fields, describing the interaction with realistic light pulses, it is impossible to find an analytic solution for Equation (2.10). Therefore, we need to use approximations in order to extract some physical phenomena. Using the dipole approximation and assuming that the interaction with the light field is weak, we can solve Equation (2.10) analytically by using perturbation theory. Although this assumption does not hold for a strong laser pulse, it is instructive to first consider this case.

Perturbation theory is widely used in physics from big scale, for example, the prediction of the famous gravitational wave arises from linearization (first order perturbation) of the space-time [11], to the small scale, for instance, people push to more than 10 dimension in string theory in order to apply perturbation theory properly [12]. Perturbation theory also gives explanations for phenomena related to single-photon and multiphoton processes. To get to the details of perturbation theory, let us recall the Schrödinger Equation (2.2), which we write here as:

$$i\hbar\frac{\partial}{\partial t}|\Psi(\mathbf{r},t)\rangle = [H_0 + V(\mathbf{r},t)]|\Psi(\mathbf{r},t)\rangle \ , \tag{2.11}$$

where H_0 is the unperturbed Hamiltonian (for example, the kinetic energy term and the Coulomb interaction between electron and core in hydrogen atom) and V is the perturbation (for example, a weak electromagnetic field). Writing

$$|\Psi(\mathbf{r},t)\rangle = e^{-\frac{iH_0t}{\hbar}}|\psi(\mathbf{r},t)\rangle \tag{2.12}$$

and inserting Equation (2.12) back in Equation (2.11), we have

$$i\hbar\frac{\partial}{\partial t}|\psi(\mathbf{r},t)\rangle = e^{\frac{iH_0t}{\hbar}}\hat{V}(\mathbf{r},t)e^{-\frac{iH_0t}{\hbar}}|\psi(\mathbf{r},t)\rangle \ . \tag{2.13}$$

If we define the change of basis for operator:

$$\tilde{V}(\mathbf{r},t) = e^{\frac{iH_0t}{\hbar}}\hat{V}(\mathbf{r},t)e^{-\frac{iH_0t}{\hbar}} \ , \tag{2.14}$$

the dynamics is described as

$$i\hbar\frac{\partial}{\partial t}|\psi(\mathbf{r},t)\rangle = \tilde{V}(\mathbf{r},t)|\psi(\mathbf{r},t)\rangle \ . \tag{2.15}$$

Equation (2.15) implies that if we have some initial unperturbed state $|I\rangle$, it propagates in time as:

$$|\psi(\mathbf{r},t)\rangle = |I\rangle + \frac{-i}{\hbar}\int_{\infty}^{t} \tilde{V}(t')|\psi(\mathbf{r},t')\rangle dt' \ . \tag{2.16}$$

To see that Equation (2.16) solves Equation (2.15), recall the Fundamental Theorem of Calculus and take the partial derivative of time. Now from Equation (2.16) we see that the unperturbed state is evolving in time, and we can define an evolution operator $\hat{T}(t)$ such that

$$\hat{T}(t) = \mathbb{1} + \frac{-i}{\hbar}\int_{\infty}^{t} \tilde{V}(t_1)\hat{T}(t_1)dt_1 \ , \tag{2.17}$$

where $\mathbb{1}$ is the identity operator. Equation (2.17) can be solved successively by substituting the expression for $\hat{T}$ into the integral on the right hand side. We obtain

$$\hat{T}(t) = \mathbb{1} + \frac{-i}{\hbar}\int_{\infty}^{t} \tilde{V}(t_1)\hat{T}(t_1)dt_1 = \mathbb{1} + \frac{-i}{\hbar}\int_{\infty}^{t} \tilde{V}(t_1)\left\{\mathbb{1} + \frac{-i}{\hbar}\int_{\infty}^{t_1} \tilde{V}(t_2)\hat{T}(t_2)dt_2\right\} dt_1 \ . \tag{2.18}$$

Repeating this step we have

$$\hat{T}(t) = \mathbb{1} + \sum_{N=1}^{\infty} \hat{T}^{[N]}(t) \ , \tag{2.19}$$

where

$$\hat{T}^{(N)}(t) = \left(-\frac{i}{\hbar}\right)^N \int_{-\infty}^{t} \tilde{V}(t_1)dt_1 \int_{-\infty}^{t_1} \tilde{V}(t_2)dt_2 \cdots \int_{-\infty}^{t_{N-1}} \tilde{V}(t_N)dt_N \ . \tag{2.20}$$

If we want to know how the Nth order term in this perturbation series for the time evolution applies to the initial state $|I\rangle$, we just use $\hat{T}^{[N]}(t)$ to obtain

$$|\psi^{(N)}(t)\rangle = \hat{T}^{(N)}(t)|I\rangle \ . \tag{2.21}$$

Moreover, we get the probability of being in some desired final state $|F\rangle$, via projection onto that state:

$$\langle F|\psi^{(N)}(t)\rangle \ . \tag{2.22}$$

For the interaction with an electromagnetic field, we can use any pair of vector potential $\mathbf{A}$ and scalar potential V from the equivalent class that corresponds to the same pair of $\mathbf{E}$ and $\mathbf{B}$. If we choose length gauge [2], we will have

$$\tilde{V}(t) = e^{\frac{iH_0t}{\hbar}}\hat{\mathbf{E}}(t)\cdot\hat{\mathbf{D}}e^{-\frac{iH_0t}{\hbar}} \ , \tag{2.23}$$

where the atomic dipole polarization operator $\hat{\mathbf{D}}$ is defined as:

$$\hat{\mathbf{D}} = -e\hat{\mathbf{r}}. \tag{2.24}$$

and

$$\hat{\mathbf{E}}(t) = \left(\frac{\hat{\mathbf{E}}}{2}e^{-i\omega_E t} + \frac{\overline{\hat{\mathbf{E}}}}{2}e^{i\omega_E t}\right) \tag{2.25}$$

Where ω_E is the frequency of the $\mathbf{E}$ field. Now we are ready to analyze the first order perturbation theory term for the interaction with an external electromagnetic field to obtain some insights into the transition between $|I\rangle$ and $|F\rangle$:

$$\begin{aligned}\langle F|\psi^{(1)}(t)\rangle &= \langle F|\hat{T}^{(1)}(t)|I\rangle = \\ &= \frac{-i}{\hbar}\left[\int_{-\infty}^{t} e^{-i(\frac{E_I}{\hbar}-\frac{E_F}{\hbar}-\omega_E)t_1}\frac{E}{2}\langle F|D|I\rangle dt_1 + \int_{-\infty}^{t} e^{-i(\frac{E_I}{\hbar}-\frac{E_F}{\hbar}+\omega_E)t_1}\frac{\overline{E}}{2}\langle F|D|I\rangle dt_1\right], \end{aligned} \tag{2.26}$$

where E_I, and E_F stand for the energy eigenvalues of $|I\rangle$ and $|F\rangle$. $D = \hat{\epsilon}\cdot\mathbf{D}$, where $\hat{\epsilon}$ represents the polarization of the light field. Taking the limit of t to ∞, we will get the first order transition amplitude as:

$$\lim_{t\to\infty}\langle F|\hat{T}^{(1)}(t)|I\rangle = \frac{-2\pi i}{\hbar}\left[\delta\left(\frac{E_I}{\hbar}-\frac{E_F}{\hbar}-\omega_E\right)\frac{E}{2}\langle F|D|I\rangle + \delta\left(\frac{E_I}{\hbar}-\frac{E_F}{\hbar}+\omega_E\right)\frac{\overline{E}}{2}\langle F|D|I\rangle\right]. \tag{2.27}$$

Those two delta functions show that the probability is non-vanishing if and only if

$$\frac{E_I}{\hbar}-\frac{E_F}{\hbar}-\omega_E = 0 \qquad \text{or} \qquad \frac{E_I}{\hbar}-\frac{E_F}{\hbar}+\omega_E = 0. \tag{2.28}$$

or

$$E_F - E_I = -\hbar\omega_E \qquad \text{or} \qquad E_F - E_I = \hbar\omega_E. \tag{2.29}$$

We realize $E_F - E_I = \pm\hbar\omega_E$ represent absorption or emission of one photon with energy $\hbar\omega_E$. We obtained one-photon transition process from the first order perturbation theory.

Thus there is a chance for an electron originally (before the interaction with the field starts) in state $|nlm\rangle$ to be found in the state $|n'l'm'\rangle$ after the end of the pulse. In other words, we see that the field can transfer some population probability from $|nlm\rangle$ to $|n'l'm'\rangle$ by absorption or emission of one photon by the atom:

$$|nlm\rangle \xrightarrow{one\ photon\ process} |n'l'm'\rangle. \tag{2.30}$$

Analyzing the matrix elements $\langle F|D|I\rangle$ one finds the following relations between the quantum numbers of the states, which are the so-called selection rules (for linearly polarized fields):

$$n' - n \neq 0, \qquad l' = l \pm 1, \qquad m' = m. \tag{2.31}$$

2.2.2 Multiphoton processes

The first order theory only works for relatively weak fields, where the expansion can be well approximated by the first order term in the Taylor expansion. But as we increase the field strength, the first order perturbation is not sufficient to explain the physical picture accurately enough and we have to use higher order terms. Analyzing the second order term $\lim_{t\to\infty}\langle F|\hat{T}^{(2)}(t)|I\rangle$ we can show that it involves terms with three Dirac delta functions (the derivation is similar to that shown above):

$$\delta\left(\frac{E_I}{\hbar} - \frac{E_F}{\hbar} + 2\omega_E\right), \qquad \delta\left(\frac{E_I}{\hbar} - \frac{E_F}{\hbar}\right), \qquad \delta\left(\frac{E_I}{\hbar} - \frac{E_F}{\hbar} - 2\omega_E\right). \tag{2.32}$$

We can see from the delta function in Equation (2.32), that the second order theory involves processes corresponding to an absorption of two photons with energy $\hbar\omega_E$ each, an emission of two photons with energy $\hbar\omega_E$, and no net absorption or emission (in this case, we need $E_I = E_F$, which says we are staying in the original state.). Moreover, we have constraints on quantum numbers in the case of the absorption and emission process as:

$$n' - n \neq 0, \qquad l' = l \pm 2, \qquad m' = m. \tag{2.33}$$

Similarly we can show for Nth order theory, we will have at most a N-photon process. Moreover, if N is an even number, the possible processes described in Nth order perturbation involve $0, 2, 4, ..., N$ photons, while if N is an odd number, the possible number of photon involved are $1, 3, 5, ..., N$. We will discuss the selection rules for multiphoton processes, specifically for the angular quantum numbers, which are central for this thesis, in Chapter 3.

2.2.3 Strong field interaction

Ever since the invention of the laser in the 1960s, lasers with higher intensities and shorter pulse durations have been developed. High intensities and ultrashort pulse durations are often related. One part of the Nobel Prize in Physics in 2018 has been recently awarded to Prof. Gerard Mourou and Prof.

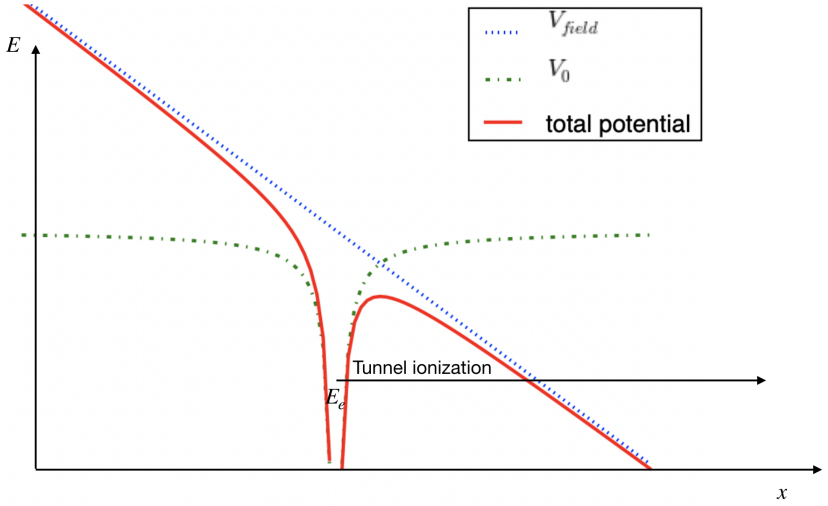

Figure 2.2: Tunneling Ionization: The blue dashed dotted line represents the Coulomb interaction potential between electron and the core, the green dotted line stands for the field potential that is applied to the atom, while the combination of those two potentials is shown by the red solid line. E_e is the energy of the electron prepared in the ground state.

Donna Strickland for their method of generating high-intensity, ultra-short optical pulses [3]. Even more recent developments have shown that high intensity lasers also open the way to generating pulses with the shortest durations to date, giving birth to the field of attosecond science (1 as = 10^{-18} s) [4, 5].

When the intensity of the field is larger than 10^{12} W/cm^2 for lasers with a wavelength in the visible or infrared regime, the strength of the interaction Hamiltonian is comparable to that of the Coulomb interaction between core and the electron, and we cannot treat the field as a perturbation anymore. This means under such strong field, the perturbation theory breaks down and we have to use other strong field theories, which revealed in the past unexpected phenomena such as High Harmonic Generation (HHG) [13, 14], Above Threshold Ionization (ATI) [15], and non-sequential double and multiple ionization [16].

We briefly discuss the strong field mechanism of tunneling ionization which also is part of the explanation for the phenomenon of HHG. As shown in Figure 2.2, under the strong field, the Coulomb potential gets greatly distorted by the external electric field and we see that there is a suppression of the potential on the positive side and enhancement on the negative side. Notice the electron's energy is still lower than the peak of the suppressed potential, but electrons have nonzero probability of being located in the continuum (the right side of the suppressed potential in the Figure 2.2); a process known as tunneling. This process cannot be described by perturbation theory. It has been long investigated, the first tunneling ionization theory formula for a static field was derived by Landau [17], an extension to oscillating electromagnetic fields was first discussed by Keldysh [18].

Tunneling ionization is the first step in the mechanism of HHG. The intuitive picture of HHG can be built by considering the process semi-classically (see Figure 2.3, [19]). First, we prepare the

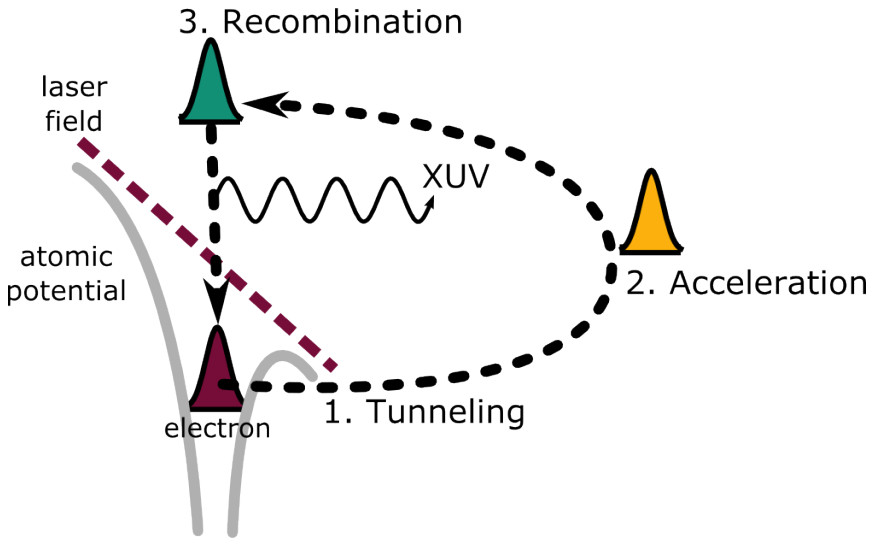

Figure 2.3: Semi-classical picture of high harmonic generation picture taken from `https://en.wikipedia.org/wiki/High_harmonic_generation`.

electron in the ground state, then through tunneling the electron is ionized and located in the continuum. While in the continuum the electron can further gain energy from the oscillating field, and return with some probability to the ion. If the electron recombines to the ground state, due to the conservation of energy' the energy in this process is released in the form of a single photon with high energy (thus high frequency). HHG was first observed in 1977 [20], for more details on HHG, see e.g. [13, 14].

Thus, we see that for the interaction with strong fields, perturbation theory is not suitable to describe the full physical picture; and in this thesis we study if the selection rules for the angular momentum, that can be derived for multiphoton processes, still hold at high intensities.

2.2.4 Numerical methods

In order to understand the dynamics of a physical system under the interaction with a strong laser pulse, we need to the solve the Time Dependent Schrödinger Equation (TDSE). Since for our system an analytical solution of the TDSE is not known, we make use of numerical solutions of the TDSE.

To this end, we have used a numerical code that is based on the Crank-Nicolson method [21] to solve the TDSE. Crank-Nicolson is a unitary, energy conservative and stable method for solving partial differential equations with second order accuracy. In general, the evolution of states governed by the Schrödinger equation can be approximated as:

$$|\Psi(\mathbf{r}, t + \Delta t)\rangle \approx e^{-i\hat{H}(t)\Delta t}|\Psi(\mathbf{r}, t)\rangle. \tag{2.34}$$

Using the Crank-Nicolson method, the time evolution operator is approximated as:

$$e^{-i\hat{H}(t)\Delta t} = \frac{1 - i\frac{\Delta t}{2}\hat{H}(t)}{1 + i\frac{\Delta t}{2}\hat{H}(t)}\,, \tag{2.35}$$

and we obtain a computationally much easier equation

$$\left(1 + i\frac{\Delta t}{2}\hat{H}(t)\right)|\Psi(\mathbf{r}, t + \Delta t)\rangle = \left(1 - i\frac{\Delta t}{2}\hat{H}(t)\right)|\Psi(\mathbf{r}, t)\rangle. \tag{2.36}$$

Thus, the Crank-Nicolson method is a finite-difference method, which solves the differential equation by approximating the derivatives as finite differences. The TDSE is then solved on a space-time grid. To obtain and represent the initial state on the grid we can use various methods, such as the spectral method [22], the random shooting method [23], or the matrix diagonalization method [24]. In the code used in this work we utilize the Krylov-Schur method provided through SLEPc as our eigensolver [25]. Moreover, in order to prevent the reflection of the wavefunction from the boundary of the spatial grid (which would cause unphysical changes in the observables), we use the exterior complex scaling (ECS) method as an absorbing boundary [26].

To obtain the results for atomic hydrogen and helium shown in this work, we have used the following parameters in our numerical calculations.

Hydrogen atom: The grid size in atomic units was (in polar coordinates) $\rho = 750$ a.u. and $z = \pm 750$ a.u. with a grid spacing of $\Delta x = 0.1$ a.u. in both directions and a time step of $\Delta t = 0.15$ a.u.

Helium atom: Here, we utilized a 450 a.u. $\times$ 900 a.u. grid with grid spacing $\Delta x = 0.1$, and time step $\Delta t = 0.15$.

Chapter 3

Results and Discussion [1]

Excitation of an atom is known to play an important role in processes induced by a strong laser pulse. Resonant enhancement in the population of excited states [27, 28, 29] and structures in the energy spectrum [30, 31, 32] and in energy-resolved angular distributions [33] of photoelectrons have been observed. These resonance effects have been explained by multiphoton absorption through Rydberg states, which are AC-Stark shifted [2] in the presence of an intense laser field. Theoretical studies of the excitation mechanism in strong fields mainly consider the distribution of the population as a function of the principal quantum number of the excited states [34, 35, 36, 37, 38]. On the other hand, analysis of the angular momentum distribution in the Rydberg states is less advanced. Predictions of Floquet theory for a monochromatic laser field [39] and results of numerical calculations for laser pulses with a trapezoidal envelope [40] yield that the angular momentum of the excited Rydberg states has the same parity as $N_p - 1$, where N_p is the minimum number of photons needed to ionize the atom. Here, we consider excitation in laser pulses with more realistic laser pulses having sine squared and Gaussian envelopes. This gives us the opportunity to study if the parity of the populated angular momentum states in such pulses agrees with the selection rules for perturbative multiphoton processes in monochromatic fields and how the results depend on laser parameters such as the pulse length and intensity.

[1] Part of the results presented also appeared in J. Venzke, R. Reiff, Z. Xue, A. Jaroń-Becker and A. Becker, *Angular momentum distribution in Rydberg states excited by a strong laser pulse*, Phys. Rev. A **98**, 043434 (2018).

3.1 Selection rules for multiphoton processes

3.1.1 Generalization of selection rules for multiphoton processes

We start our study by generalizing the selection rule, discussed above for single photon excitation, to the multiphoton process. In the perturbative regime, we just to apply the single photon selection rule successively. Thus, the multiphoton selection rule leads to a change in the quantum numbers n, l, m for N_p-photon absorption process as follows:

$$E_{n'} - E_n = N_p \hbar\omega_E \ , \tag{3.1}$$

$$|l' - l| = \begin{cases} 1, 3, 5, ..., N_p, & \text{for odd number of photons} \\ 0, 2, 4, 6, ..., N_p, & \text{for even number of photons} \ , \end{cases} \tag{3.2}$$

and

$$m' - m = 0. \tag{3.3}$$

Since under the influence of a strong field, the interaction with the field becomes highly nonlinear and perturbation theory no longer works well, we want to know whether or not the above selection rule still applies. To this end, we have to consider that in a strong laser field the highly excited states are shifted. To figure out the number of photons corresponding to a certain transition for a given intensity and frequency, we assume that the energy shift of high-lying excited states under the influence of an intense laser field is approximately equal to the ponderomotive shift [32] and the shift occurs instantaneously during the pulse [41]. The number of N_p photon process for a laser pulse with peak intensity I and central frequency field ω_E is determined by the resonance condition:

$$I = 4\omega_E^2 (N_p \omega_E + E_i - E_n) \ , \tag{3.4}$$

where E_i is the energy of the initial state and E_n is the exited state energy we want to be in resonance with. Using the ground state of the atom as the initial state to be e.g. the $n = 8$ state (E_8), the photon number is given by

$$N_p = \frac{I + 4(E_8 - E_0)\omega_E^2}{4\omega_E^3} \ , \tag{3.5}$$

where E_0 is the atomic ground state energy.

In our calculations we have considered peak intensities such that the $n = 8$ states of an atom are in resonance at a central frequency ω_E with different number of photons N_p. Since we study the interaction

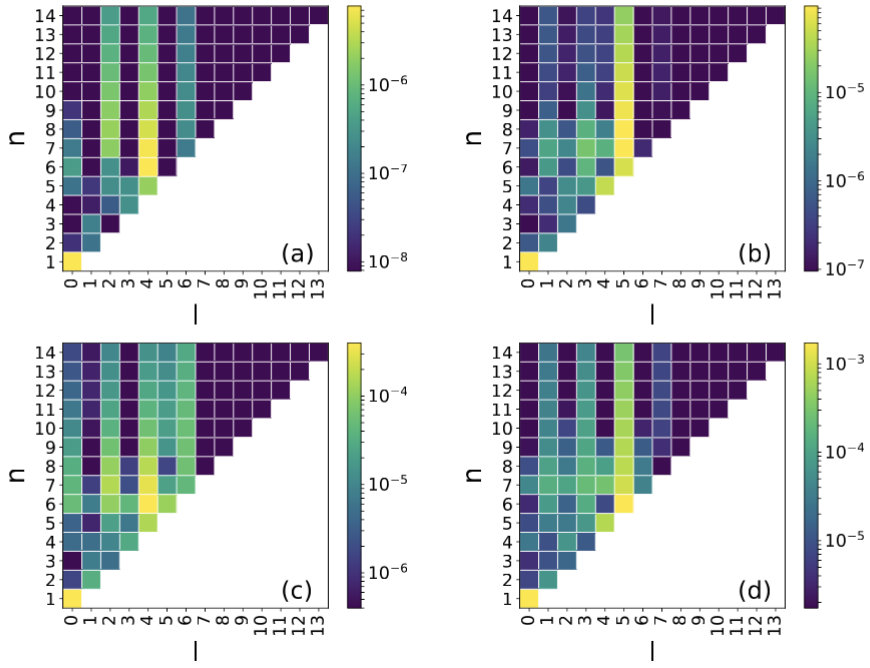

Figure 3.1: Excited state distribution in hydrogen atom as function of n (vertical axis) and l (horizontal axis) at the end of 20 cycle pulses with sin squared envelope and peak intensities: (a) $I_0 = 3.4 \times 10^{13}$ W/cm^2, (b) $I_0 = 6.0 \times 10^{13}$ W/cm^2, (c) $I_0 = 8.6 \times 10^{13}$ W/cm^2, and (d) $I_0 = 1.12 \times 10^{14}$ W/cm^2. Left (right) column corresponds to cases in which the Rydberg states are resonant with an even (odd) number of photons.

with laser pulses, instead of monochromatic fields, more than one manifold of states can be resonantly excited. For example, for hydrogen atom the bandwidth of a 20 cycle sine squared pulse at 800 nm covers all excited states $n \gtrapprox 6$ within the same N_p photon process. We further note that for hydrogen atom, the $n = 3$ and $n = 2$ states are approximately resonant via $N_p - 1$ and $N_p - 2$ photon processes, respectively, assuming that the energy shift of these states equals the ponderomotive shift as well.

3.1.2 Selection rules: Parity effect in interaction with pulses

We first study the angular momentum distribution in Rydberg states of the hydrogen atom. The population in each quantum state (n, l) at the end of the pulse is shown in Fig. 3.1 (20 cycle pulses with sine-squared envelope) and Fig. 3.2 (14 FWHM cycle pulses with Gaussian envelope) for peak intensities between 10^{13} and 10^{14} W/cm^2. In the results we indeed observe signatures of the selection rules resulting in dominant population of states with an even (odd) angular momentum quantum number for the absorption of even (odd) photons in the plots on the left (right). This shows that in the intensity regime of 10^{13} to 10^{14} W/cm^2 the multiphoton selection rules are effective for long pulses of about 20 cycles. Furthermore, we see that the parity effect is found to occur independent of the form of the envelope. We therefore restrict ourselves below to pulses with a sine-squared envelope.

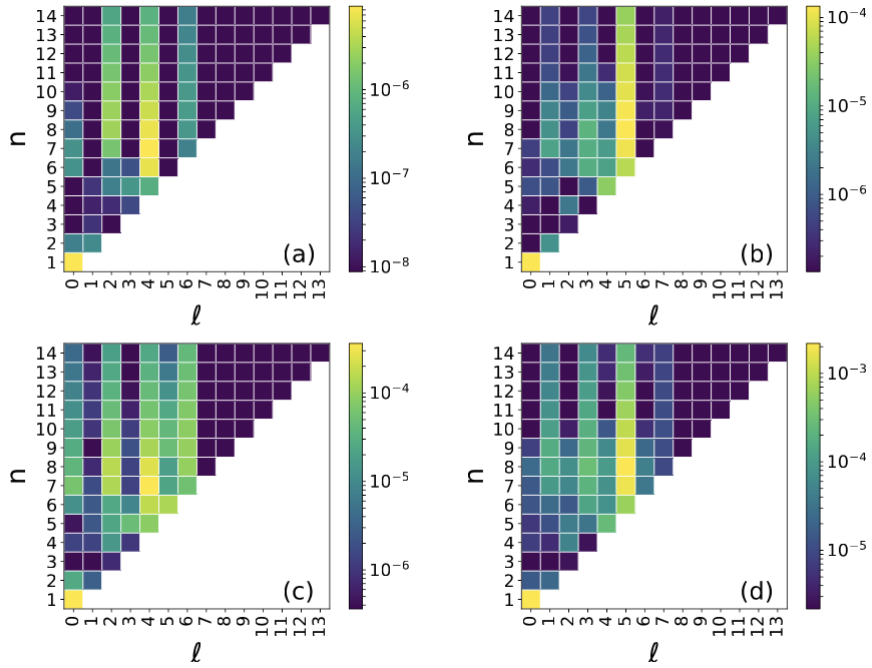

Figure 3.2: Same as Fig. 3.1 but for pulses with Gaussian envelope and 14 cycles FWHM. The pulse duration approximately matches that for the sine-squared pulses in Fig. 3.1 at FWHM.

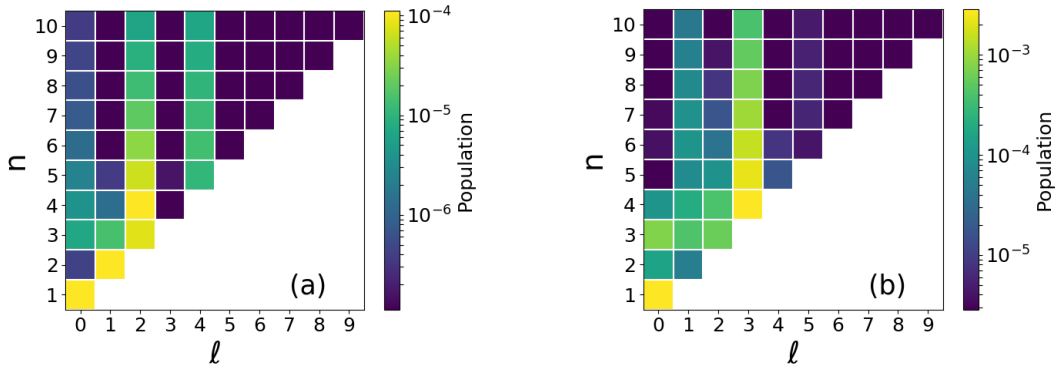

Figure 3.3: Excited state distribution in helium atom as function of n (vertical axis) and l (horizontal axis) at (a) 267 nm and peak intensity of 5.0×10^{14} W/cm^2 (6 photon process), and (b) 267 nm with peak intensity of 1.2×10^{15}W/cm^2 (7 photon process) of a 10-cycle laser pulse.

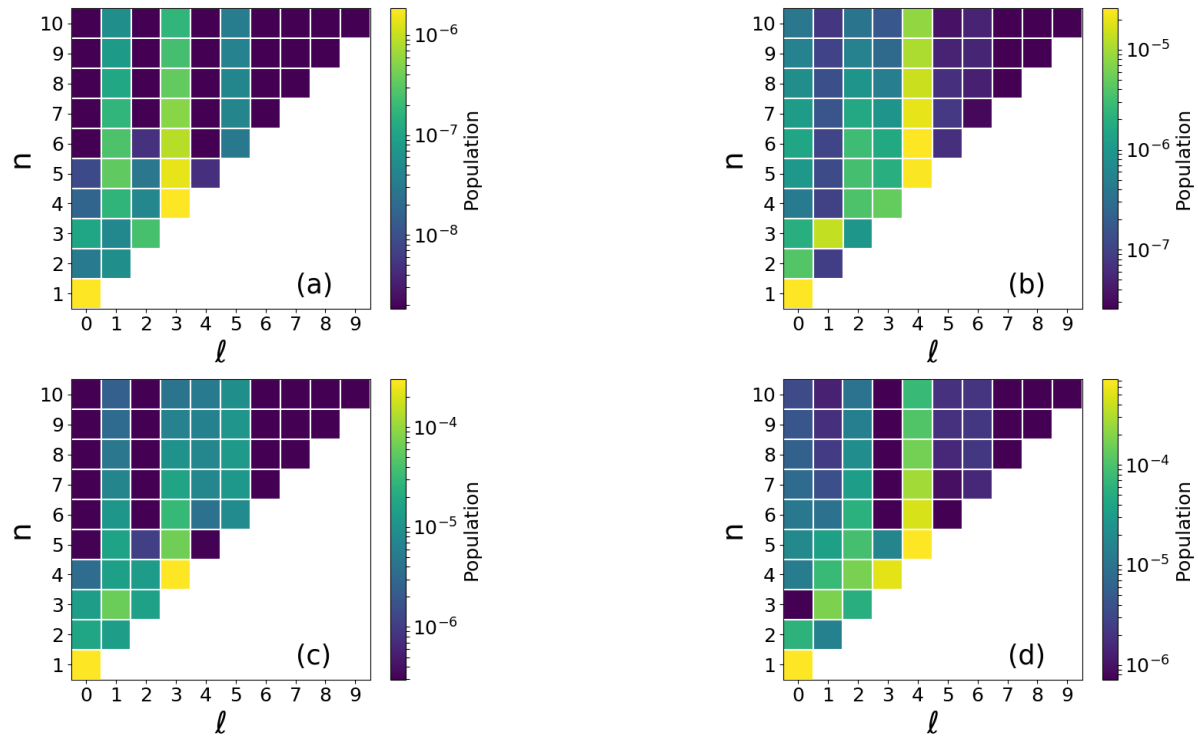

Figure 3.4: Same as Fig. 3.3 but for laser pulses at (a) 400 nm with intensity of 2.3×10^{14} W/cm^2 (9 photon process), (b) 400 nm with intensity 4.4×10^{14} W/cm^2 (10 photon process), (c) 400 nm with intensity 6.5×10^{14} W/cm^2 (11 photon process), (d) 400 nm with intensity 8.6×10^{14} W/cm^2 (12 photon process).

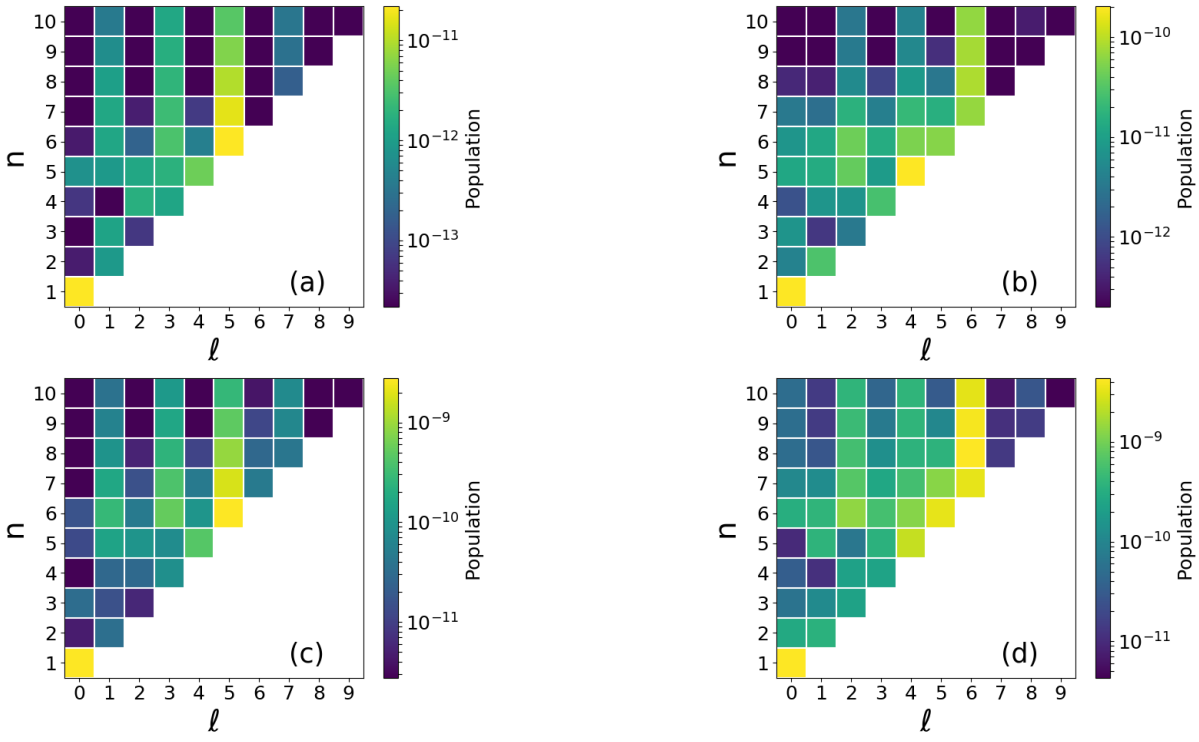

Figure 3.5: Same as Fig. 3.3 but for laser pulses at (a) 800 nm with intensity 8.3×10^{13} W/cm^2 (19 photon process), (b) 800 nm with intensity 1.1×10^{14} W/cm^2 (20 photon process), (c) 800 nm with intensity 1.4×10^{14} W/cm^2 (21 photon process), (d) 800 nm with intensity 1.6×10^{14} W/cm^2 (22 photon process).

We further confirm the selection rule by studying the angular momentum population distribution in helium atom excited with 10 cycles sin squared pulses with various frequencies and intensities. The numerical results are presented in Figs. 3.3 - 3.5. From those results, we can see that the multiphoton selection rule applies in general: For odd number photon process there is suppression in the population of states with even l number and enhancement for those with odd l number. In contrast, for even number photon processes there exists a suppression for states with odd l number and an enhancement for those with even l number. In particular, for odd photon processes Fig. 3.4 (a) shows excited states with $l = 1, 3, 5$ populated while population in the states with $l = 0, 2, 4$ are strongly suppressed, and for even photon processes, there results presented in Fig. 3.3 (a) clearly reveal that the $l = 2, 4$-states got populated and the other l-states are suppressed. A potential explanation why $l = 0$ state got suppressed even for the even photon number process will be given later in the report.

3.1.3 Dependence on intensity and pulse length

To investigate the domain over which multiphoton selection rules, that are derived from perturbation theory, can be used in the non-perturbative regime, we have to study the excitation process at different intensities and pulse lengths. From the results in Figs. 3.3 - 3.5, most specifically those at 800 nm, we can see that for increasing intensity of the field, the population distribution begins to blur. The contrast between the population in even and odd l-states gets less strong and so the selection rule appears to be no longer valid. This is because the energy of the states shifts with the ponderomotive energy $U_p \propto \frac{I}{\omega_E^2}$, which increases with increasing intensity and hence varies over the pulse. So, during the rising and falling edges of the pulse, a particular energy level will shift several times in resonance for odd as well as even number photon process. Thus, the shift of the energy level is rather dynamic and complex at high intensities and each state can be resonantly populated once or several times during the pulse. Consequently, odd and even l-states get populated and for the overall distribution at the end of the pulse the selection rule does not longer apply. Moreover, we see that the population distribution with highest intensity for 800 nm is more blurred out than the population distribution with highest intensity for 400 nm. This is because 800 nm field has lower frequency ω_E than 400 nm field, therefore larger shift (approximated by the ponderomotive energy $U_p \propto \frac{I}{\omega_E^2}$) of states is expected for 800 nm than 400 nm field. Since the shift of states for 800 nm field is stronger, the states will be more often in resonance over the course of the pulse than for a 400 nm pulse. Consequently, the contrast due to population in odd vs. even number photon process is less strong at the longer wavelength and we see more blurred out population distribution for 800 nm than 400 nm.

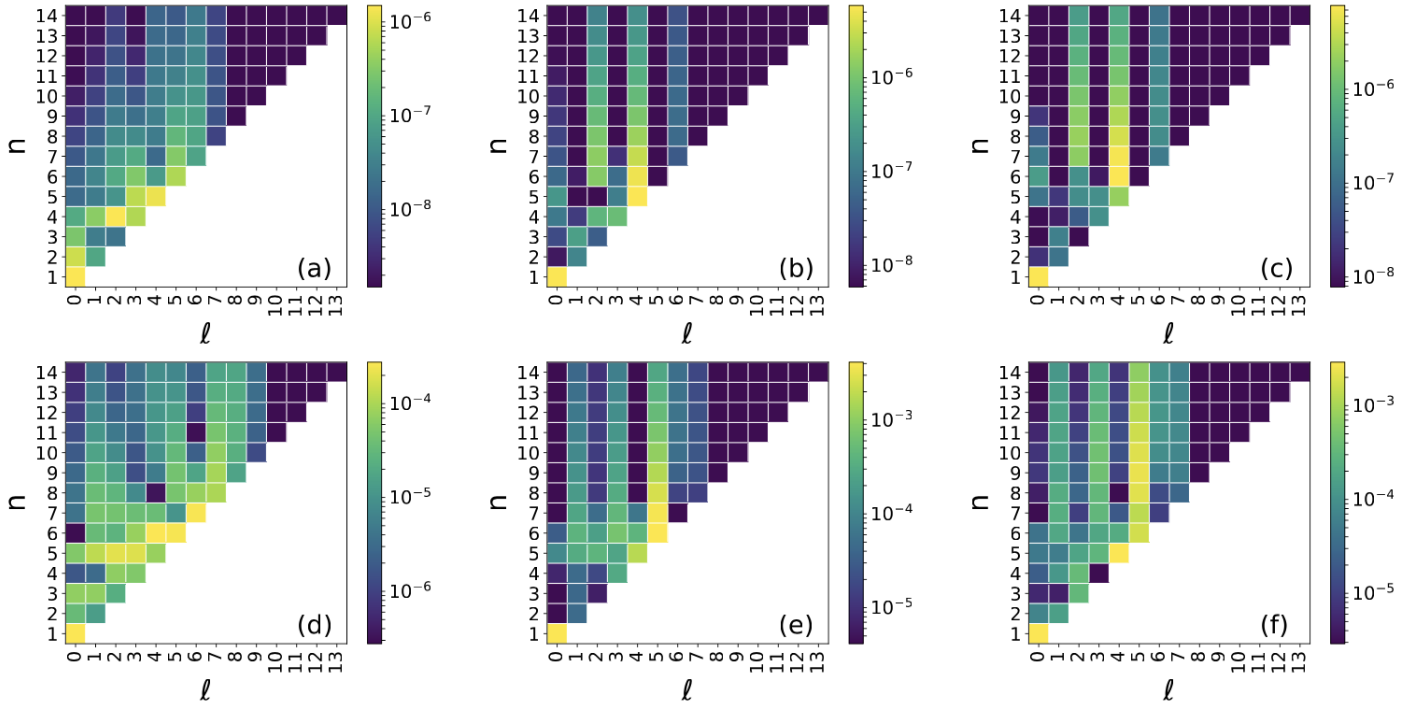

Figure 3.6: (Color online) Excited state distribution as function of l (horizontal axis) and n (vertical axis) at the end of 2 cycle (panels on the left), 10 cycle (panels in middle), and 20 cycle (panels on right) pulses, at low peak intensity $I_0 = 3.4 \times 10^{13}$ W/cm^2(top row), and high peak intensity $I_0 = 1.64 \times 10^{14}$ W/cm^2(bottom row).

We further have studied how the angular momentum distribution varies with the number of cycles at a given peak intensity. The results of our calculations for the effect of pulse length on population distribution are shown in Fig. 3.6. The time-frequency uncertainty relation yields that a pulse spectrum broadens as the number of optical cycles decreases. Consequently, in an ultrashort pulse an excited state can be reached via absorption of different number of photons. Due to this mix of even and odd number of photon processes one may expect that in such pulses a separation in population of odd vs. even angular momentum quantum states cannot be achieved. This is confirmed by the results of our numerical calculations at low and high intensities, shown in Fig. 3.6(a) and (d). For a 2 cycle pulse there is a smooth distribution over the lower angular momentum states for each principal quantum number at low (3.4×10^{13} W/cm^2, panel (a)) and high (1.64×10^{14} W/cm^2, panel (d)) peak intensity.

In contrast, the narrowing of the energy spectrum as pulse duration increases does not necessarily lead to an increase of the population in the angular momentum states that are allowed by the multiphoton selection rule. For the low intensity 10-photon resonant process (3.4×10^{13} W/cm^2, Fig. 3.6, upper row) we observe that Rydberg states start to be populated based on the multiphoton selection rule when the pulse duration is increased to 10 and 20 cycles. On the other hand, at the higher intensity (1.64×10^{14} W/cm^2, Fig. 3.6, lower row) we observe the states are not following the multiphoton selection rule.

Within the interpretation of resonant excitation the loss of the multiphoton selection rule effect

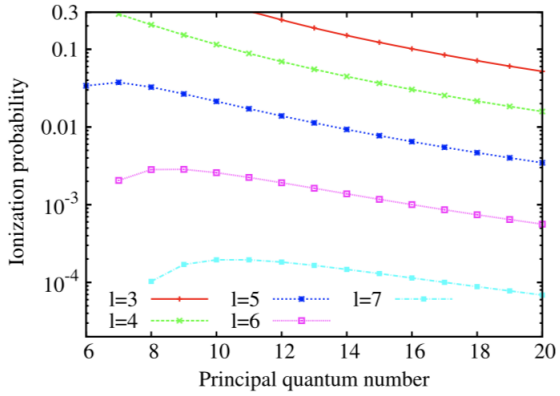

Figure 3.7: The ionization probability for the absorption of one 800 nm photon for a flat-top pulse of 5 fs duration at the intensity of 10^{14} W/cm^2 calculated using first-order perturbation theory. Note that the probability scales linearly with laser intensity and pulse duration in this model. Figure taken from [35].

for long pulses with high peak intensities can be understood as follows. As mentioned above, at the higher peak intensity the highly excited states are shifted into resonance for 10 - 14 photon processes over the rising and trailing parts of the pulse, before they are resonantly excited with a 15 photon process at the peak intensity. Although the excitation probability raises with an increase of the intensity during the pulse, the time intervals over which the states are in resonance with a certain photon-order process increase with the pulse length. Thus, there is a significant excitation of the Rydberg states due to the absorption of odd as well as even numbers of photons in a pulse at high peak intensity and long duration. Furthermore, excitation channels driven by absorption of different numbers of photons with the same parity may interfere, leading to the enhancement or suppression of population in certain angular momentum states and the loss of the parity effect. Interference effects in excitation have been studied extensively in the few-photon regime [42, 43, 44, 45, 46].

3.2 Population trapping

3.2.1 Resistance to ionization for high l states

In Figures 3.1 - 3.6, we see that the high angular momentum states ($l > 7$) are not much populated for all cases, in agreement with previous studies [47] and semi-classical estimates [48]. We also see that the low l states are not populated, this is in agreement with the results presented by Li et al. [35], who conjectured that electrons in the low angular momentum states more easily absorb additional photons resulting in suppression of population in these states due to ionization. They showed (Figure 3.7) by using first order perturbation theory that as l increases, the ionization probability decreases. The reason for this trapping of population is that lower-n and lower-l states that can be efficiently

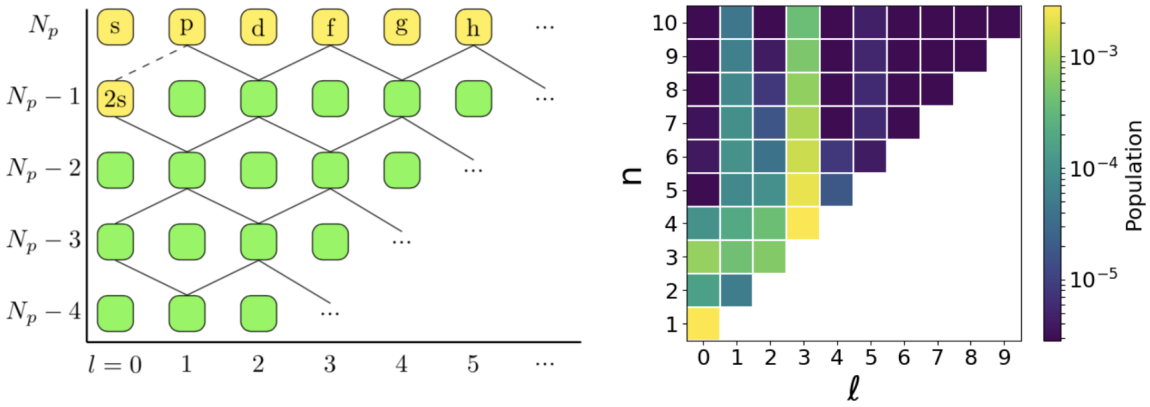

Figure 3.8: The absorption pathways (left) and population distribution (right) at 270 nm and peak intensity $I = 1.2 \times 10^{15}$ W/cm^2 field (7 photon process). In the absorption pathway picture, green squares represent virtual states with energy $N\omega_E$ above the ground state and angular momentum l. The yellow squares represent real states labeled by the quantum numbers. Solid lines refer to open pathways while dashed lines represent pathways which are suppressed due to population trapping in a lower excited state.

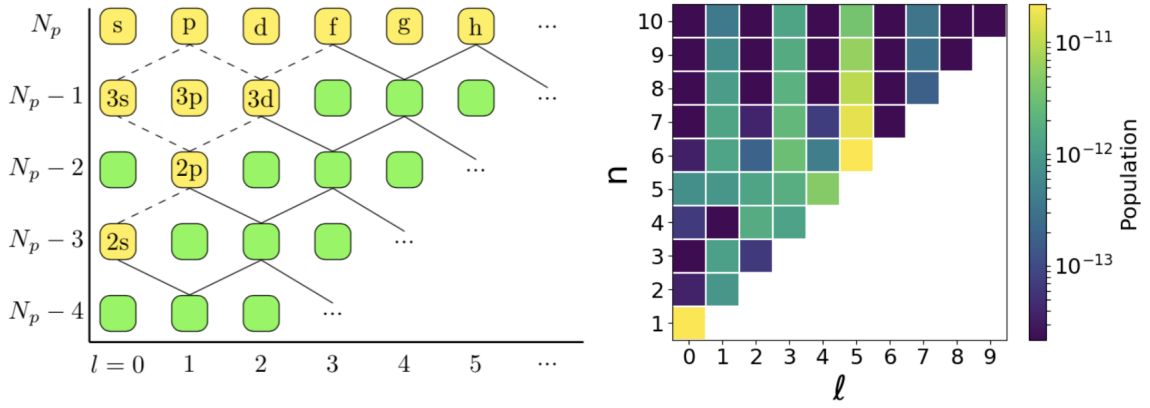

Figure 3.9: Same as Figure 2.12 but for 800 nm with intensity $I = 8.3 \times 10^{13}$ W/cm^2 field (19 photon process).

tunnel ionized. In contrast, high-n, high-l Rydberg states can only be eliminated through multiphoton ionization (according to Keldysh theory [49]). However, since the electron density in these states is located far enough from the core of the atom the electron behaves like a free electron, which do not absorb photons. Therefore electron in states with high angular momentum resist ionization and cause the population to be trapped in high-n, high-l states.

3.2.2 Trapping in lower excited states

In general, in our results for an odd parity process (right column of Figure 3.1 and Figure 3.2) predominantly one angular momentum state ($l = 5$) is populated. This is in agreement with the mechanism presented by Li et al. [35]. However, our results (left column of Figure 3.1 and Figure 3.2) for even parity processes exhibit a pattern, alternating in l, showing that both low and high angular

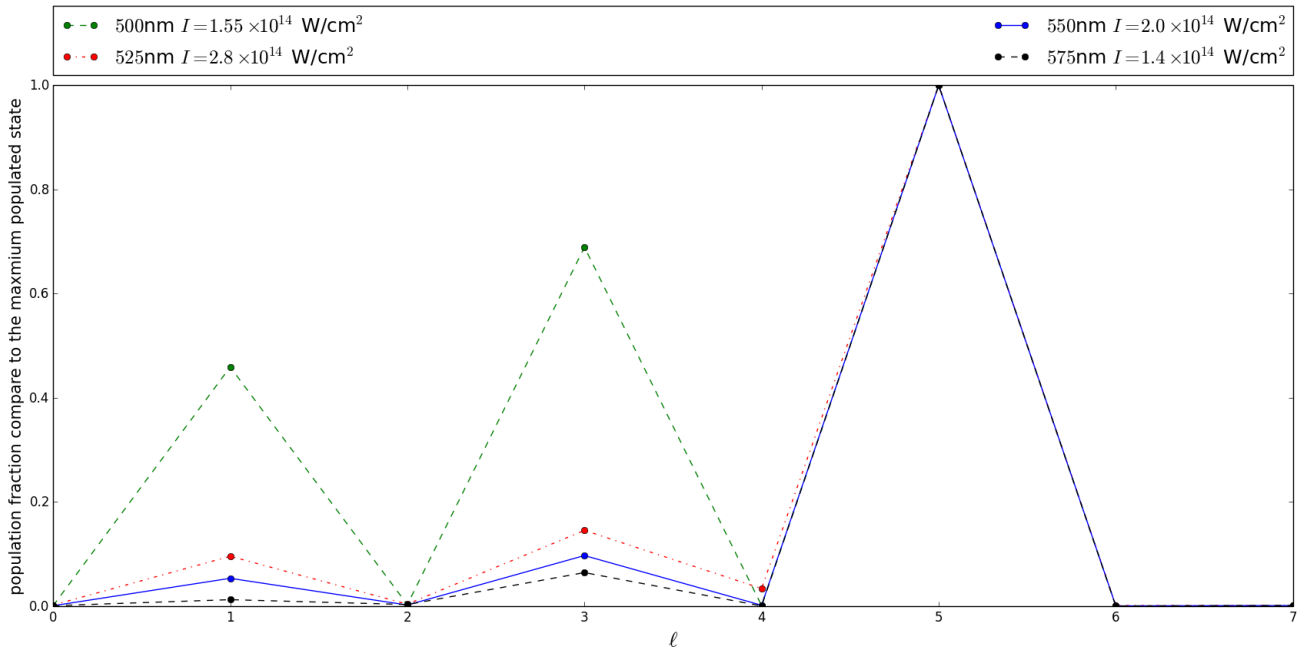

Figure 3.10: Population in 8l states (normalized to the population in the $l = 5$, the most populated state) for the interaction of helium atom with 10-cycle laser pulse at various wavelengths. Green dashed line: 500 nm, 1.55×10^{14} W/cm^2 field; red dashed dotted line: 525 nm, 2.8×10^{14} W/cm^2 field, blue solid line: 550 nm, 2.0×10^{14} W/cm^2 field, and black dotted line: 575 nm, 1.4×10^{14} W/cm^2 field.

momentum states, except for the s-states, remain populated at the end of the pulse.

Therefore we propose an alternative explanation. In the Figures 3.8 and 3.9, the panels on the left show the various pathways leading to a resonant population in the Rydberg states for helium atom upon absorption of N_p photons in an even or odd photon process. The yellow squares represent real states labeled by their quantum numbers while the empty green states represent virtual states. Starting from the 1s ground state, the absorption of successive photons proceeds through virtual states. If the population reaches any real state via resonance (that is, the energy difference between states are equal to several $\hbar\omega_E$), then we assume that part of the population will be trapped during the pulse and the further pathway will be suppressed. Solid lines refer to open pathways while dashed lines represent pathways which are suppressed due to population trapping in the lower excited states. We use Equation (3.4) to predict which state is in resonance.

This trapping picture can explain most of the results for the population distributions we have obtained. For example, in Figure 3.8, the 2s state is resonant with $N_p - 1$ photon process. Hence, the further pathway to p states will be suppressed, and indeed we see in the population plot (on the right) that p-states ($l = 1$) for large n are partly suppressed. It appears that this mechanism can also explain the results in Figure 3.9, where the pathways leading to Rydberg p-states are both suppressed and one of the two pathways to the f-states are suppressed. We therefore expect that the population in the

p-states (for large n) will be more suppressed than that in the f-states, and both of them should be less populated than the h-states. Indeed, we see this in the population plot on the right.

Moreover, based on the number of total pathways leading to states with a given angular momentum, we can explain why we observe, in general, that s-states are always suppressed even for the even number photon process. As one can see from our diagrams there are less pathways to s-states than to those with higher angular momentum. As a result, it is likely that the population of s-state is suppressed due to the lack of absorption pathways.

To further explore the proposed trapping mechanism, we have studied the change in the population as we change the wavelength of the laser. Using Equation (3.4), we expect that if we increase the laser wavelength (i.e., decrease the frequency) from 500 nm to 575 nm for interaction with helium atom, the $3s$ and $3d$ state will shift more and more into resonance with the laser field. Thus, according to our picture more population will be trapped in the $3s$ and $3d$ states for an increase of the wavelength, which will lead to a suppression of the pathways to the Rydberg p- and f-states. In our results we indeed see this suppression in the p- and f-states for the $n = 8$ state in helium atom, when the wavelength is changed from 500 nm to 575 nm (Figure 3.10). The intensities are adjusted to ensure resonance with the $n = 8$ manifold in helium atom.

Chapter 4

Summary and future goals

We have analyzed the angular momentum distribution in the Rydberg states of hydrogen atom and helium atom excited by short strong laser pulses, based on numerical results of the time dependent Schrödinger equation, which we solved using a second order Crank-Nicolson scheme. At low intensities the pattern in the population across the angular momentum states can be explained via a parity effect due to the selection rules in multiphoton absorption along with the suppression of pathways due to population trapping in low excited states, if the applied laser pulse is not too short. At high intensities the parity effect gets lost even for long pulses, potentially since the Rydberg states are in resonance with photon processes of different orders for a significant time during the rising and trailing parts of the pulse.

In this work, we only tested multiphoton selection rules for the interaction with linearly polarized pulses; in future work we also are interested in studying the multiphoton selection rules for other kinds of pulses such as circularly and elliptically polarized fields. For the proposed trapping mechanism, we did not provide a mechanism under which conditions part of the population for any real state in the pathway may be trapped during the pulse. Thus, a future goal is to address this question in more detail to further understand the suppression of population in certain angular momentum states. Furthermore, the shift of a state is, in general, very dynamic and highly dependent on the parameters of the field. In this work we assumed that each state shifts with the ponderomotive energy, which may not be sufficient enough to describe the real physical situation. Thus, finding a more systematic state shifting scheme will be crucial for further studies of the proposed trapping mechanism and potential applications. In fact, we plan to use Floquet theory [50] to investigate the shift of states in a more accurate way.

Bibliography

[1] P. A. M. Dirac, *The Principles of Quantum Mechanics*, University Press, Oxford, (1948).

[2] B. H. Bransden, C. J. Joachain, *Physics of atom and molecules*, chapter 4.3, Longman Scientific Technical, (1983).

[3] `https://www.nobelprize.org/prizes/physics/2018/summary/`

[4] P. M. Paul, E. S. Toma, P. Breger, G. Mullot, F. Augé, Ph. Balcou, H. G. Muller, and P. Agostini, *Science*, 292, 1689 (2001).

[5] M. Hentschel, R. Kienberger, Ch. Spielmann, G. A. Reider, N. Milosevic, T. Brabec, P. Corkum, U. Heinzmann, M. Drescher, F. Krausz. *Nature* **414**, 509, (2001).

[6] P. Auger, *Compt. Rend.* (Paris) 177, 169 (1923).

[7] U. Fano, *Phys. Rev.* 124, 1866 (1961).

[8] S. Weinberg, *Lectures on Quantum Mechanics*, Cambridge University Press (2015).

[9] J. D. Jackson, *Classical Electrodynamics*,chatper 11, John Wiley & Sons, INC. (1998).

[10] R. Shankar, *Principles of Quantum Mechanics*, Plenum Press, New York, (1994).

[11] C. W. Misner, K. S. Thorne, J. A. Wheeler, *Gravitation*, W. H. Freeman, (1973).

[12] Weinstein, Steven and Rickles, Dean, *Quantum Gravity*, The Stanford Encyclopedia of Philosophy (Summer 2018 Edition), Edward N. Zalta (ed.), `https://plato.stanford.edu/archives/sum2018/entries/quantum-gravity/`.

[13] D. B. Milosevic, W. Becker, and R. Kopold. Generation of circularly polarized high-order harmonics by two-color coplanar field mixing. *Phys. Rev. A*, 61(6), (2000).

[14] M. Lewenstein, Ph. Balcou, M. Yu. Ivanov, Anne L'Huillier, and P. B. Corkum. Intense few-cycle laser fields: Frontiers of nonlinear optics. *Phys. Rev. A*, 49(2117), (1994).

[15] P. Agostini, F. Fabre, G. Mainfray, G. Petite and N.K. Rahman,*Phys. Rev. Letters* **42**, 1127, (1979).

[16] B. Walker, B. Sheehy, L. F. DiMauro, P. Agostini, K. J. Schafer, and K. C. Kulander, *Phys. Rev. Lett.* 73, 1227 (1994).

[17] L.D. Landau and E.M. Lifshitz, *Quantum Mechanics*, Pergamon, New York, 2nd ed., pg, 276, (1965).

[18] L. V. Keldysh *Sov. Phys*, JETP **20**:1307, (1965).

[19] P. B. Corkum. Plasma Persepctive on Strong Field Multiphoton Ionization. *Phys. Rev. Lett.*, 71 (13), (1993).

[20] N. H. Burnett, H. A. Baldis, M. C. Richardson, and G. D. Enright. Harmonic generation in CO2 laser target interaction, *Appl. Phys. Lett* 31, 172 (1977).

[21] J. Crank, P, Nicolson, *A practical method for numerical evaluation of solutions of partial differential equations of the head conduction type*, Proc. Camb. Phil. Soc. 43 (1), (1947).

[22] M. D. Feit, J. A. Fleck Jr., A Steiger. *Journal of computational Physics*, 47:412, (1982).

[23] W. H. Press. *Numerical Recipes: The Art of Scientific Computing.* Cambridge University Press, (2007).

[24] T. A. Beu. *introduction to Numerical Programming: A Practical Guide for Scientists and Engineers Using Python and C/C++.* CRC Press, (2014).

[25] *SLEPc Users Manual Scalable Library for Eigenvalue Problem Computations* http://slepc.upv.es/documentation/slepc.pdf.

[26] F. He, C. Ruiz, and A. Becker, *Phys. Rev.* A 75, 053407, (2007).

[27] M. Chini, X. Wang, Y. Cheng, H. Wang, Y. Wu, E. Cunningham, P.-C. Li, J. Heslar, D.A. Telnow, S.-I Chu, and Z. Chang, *Nat. Photon.* **8**, 437 (2014).

[28] S. Camp, K.J. Schafer, and M.B. Gaarde, *Phys. Rev. A*, **92**, 013404 (2015).

[29] E.S. Toma, Ph. Antoine, A. de Bohan, and H.G. Muller, J. *Phys. B: At. Mol. Opt. Phys.* **32**, 5843 (1999).

[30] R.R. Freeman, P.H. Bucksbaum, H. Milchberg, S. Darack, D. Schumacher, and M.E. Geusic, *Phys. Rev. Lett.*,**59**, 1092 (1987).

[31] M.D. Perry, A. Szoke, and K.C. Kulander, *Phys. Rev. Lett.*, **63**, 1058.

[32] P. Agostini, P. Breger, A. L'Huillier, H.G. Muller, G. Petite, A. Antonetti, and A. Migus, ,*Phys. Rev. Lett.* **63**, 2208 (1989).

[33] H. Rottke, B. Wolff-Rottke, D. Feldmann, K.H. Welge, M. Dörr, R.M. Potvliege, and R. Shakeshaft, *Phys. Rev. A*, **49**, 4837 (1994).

[34] Q. Li, X.-M. Tong, T. Morishita, H. Wei, and C.D. Lin, *Phys. Rev. A*, **89**, 023421 (2014).

[35] Q. Li, X.-M. Tong, T. Morishita, C. Jin, H. Wei, and C.D. Lin, *J. Phys. B: At. Mol. Opt. Phys.* **47**, 204019 (2014).

[36] H. Zimmermann, J. Buller, S. Eilzer, and U. Eichmann, *Phys. Rev. Lett.*, **114**, 123003 (2015).

[37] W.-H. Xiong, X.-R. Xiao, L.Y. Peng, and Q. Gong, *Phys. Rev. A*, **94**, 013417 (2016).

[38] S. Beaulieu, S. Camp, D. Descamps, A. Comby, V. Wanie, S. Petit, F. Legare, K.J. Schafer, M.B. Gaarde, F. Catoire, and Y. Mairesse, *Phys. Rev. Lett.*, **117**, 203001 (2016).

[39] K. Krajewska, I.I. Fabrikant, and A.F. Starace, *Phys. Rev. A*, **86**, 053410 (2012).

[40] M. V. Fedorov, *Laser Phys.* **3** 219, (1993).

[41] F. He, C. Ruiz, A. Becker, and U. Thumm, *J. Phys. B: At. Mol. Opt.* **44**, 211001 (2011).

[42] H.L. Kim, R. Bersohn *J. Chem. Phys.*, 107, p. 4546, (1997).

[43] Y. Yin, C. Chen, D.S. Elliott, A.V. Smith *Phys. Rev. Lett.*, 69 , p. 2353, (1992).

[44] B. Sheehy, B. Walker, L.F. DiMauro *Phys. Rev. Lett.*, 74, p. 4799,(1995).

[45] E. Dupont, P.B. Corkum, H.C. Liu, M. Buchanan, Z.R. Wasilewski *Phys. Rev. Lett.*, 74, p. 3596, (1995).

[46] A. Hache, Y. Kostoulas, R. Atanasov, J.L.P. Hughes, J.E. Sipe, H.M. van Driel *Phys. Rev. Lett.*, 78, p. 306, (1997).

[47] B. Piraux, F. Mota-Furtado, P.F. O'Mahony, A. Galstyan, and Yu. V. Popov, *Phys. Rev. A.*, **96**, 043402 (2017).

[48] D.G. Arbo, K.I. Dimitriou, E. Persson, and J. Burgdörfer, *Phys. Rev. A.* **78**, 013406 (2008).

[49] S. V. Popruzhenko *J. Phys. B: At. Mol. Opt. Phys.* **47** 204001, (2014).

[50] F. H. M. Faisal, *Theory of multiphoton process*, Plenum Press, New York, (1987).